

The Redshift Evolution of Λ CDM Halo Parameters

Juan Carlos Muñoz-Cuartas^{*a}, Andrea Macciò^b, Stefan Gottlöber^a, Aaron Dutton^{c†}

^a*Astrophysikalisches Institut Potsdam*

^b*Max Planck Institut Für Astronomie*

^c*Department of Physics and Astronomy, University of Victoria*

E-mail: jcmunoz@aip.de

We study the mass and redshift dependence of the concentration parameter in Nbody simulations spanning masses from $10^{10}h^{-1}M_{\odot}$ to $10^{15}h^{-1}M_{\odot}$ and redshifts from 0 to 2. We present a series of fitting formulas that accurately describe the time evolution of the concentration-mass relation since $z=2$. Using arguments based on the spherical collapse model we study the behaviour of the scale length of the density profile during the assembly history of haloes, obtaining physical insights on the origin of the observed time evolution of the concentration mass relation. We present preliminary results of the implementation of this model in the prediction of the values of the concentration parameter for different masses and redshifts.

Cosmic Radiation Fields: Sources in the early Universe
November 9-12, 2010
Desy, Germany

*Speaker.

†CITA National Fellow.

1. Introduction

The current standard cosmological paradigm, the so called Λ CDM universe, establishes that the universe has a spatially flat geometry whose dynamics is nowadays dominated by dark energy with a minor contribution from the dark matter, both of them are of unknown nature and where neither radiation nor baryonic matter play an important role in the present dynamical state of the universe. In this scenario, structures grow as gravitational instabilities in the dark matter density field where the first objects are the smaller ones and subsequent mergers and accretion of the small objects on to the big ones lead to a hierarchical scenario of growth of structures. Galaxies are supposed to form as gas accretes and cools down in the gravitational potential well of those previously formed dark matter haloes [20]. Dark matter haloes play a crucial role in the study of the formation of galaxies and the evolution of the universe, they provide the environment where baryons can cool down to form stellar systems, which finally are the objects we can observe in the universe and are the ones responsables for much of the cosmic radiation field we can account for.

The properties of dark matter haloes can be characterized with several different parameters, one of the most important ones is the concentration parameter which accounts for the shape of the mass density profile and therefore has important implications in determining the properties of the galaxies forming inside [12], as well as it has direct influence in the flux of radiation produced during the annihilation process of dark matter in the center of the halo [7]. Previous works have been addressed in the study of the structure of dark matter haloes. [15] (NFW) proposed that the characteristic density of dark matter haloes was directly proportional to the density of the universe at time of formation, making possible to connect today properties of the dark matter density profile to the halo formation history and to the evolution of the expanding universe. [3] and [4] have studied the mass dependence of the concentration parameter, they found a power law mass dependence of the concentration parameter that scales in time with scale factor. [19] found a strong correlation between the concentration parameter and the mass accretion history of haloes, and confirmed the claims of NFW and [3] where the concentration of the halo is related to their definition of time of formation of the halo. [6] investigated the power spectrum dependence of the concentration parameter. [21],[22],[23] re-addressed the problem of the properties of the halo mass distribution and studied the connection between the mass accretion history (MAH) and the concentration parameter using a large suite of simulations. They found a relation between the scale length of the halo r_s and the mass interior to that radius M_s . Using that relation in his model for the MAH and an appropriated choice of the time of transition between the two different modes of accretion enabled them to model the mass and redshift dependence of the concentration parameter. [10] and [11] have studied the cosmology and mass dependence of the concentration, shape and spin parameters at $z=0$ and revised the models of NFW and [3]. In [13] we studied the mass and redshift dependence of spin, shape and concentration parameters for a WMAP5 cosmology and found the evolution of the concentration parameter to be due to the evolution of the inner halo mass distribution (inside r_s) and suggest that this evolution can be modeled as a spherical perturbation growing in the inner region of the halo. This description gives physical insight in to the understanding of the mass and redshift dependence of the concentration parameter.

In this work we present in more detail those results presented in [13] and focus on the redshift dependence of the concentration parameter. We show our advances in the implementation of those

ideas in the construction of a model able to make predictions for the values of the concentration parameter for different masses and redshifts, this may be important for the modeling of the properties of galaxies as well as for the study of sources of annihilation of dark matter in the early universe.

2. Simulations and methods

2.1 Simulations

All simulations in this work have been performed with PKDGRAV, a tree code written by Joachim Stadel and Thomas Quinn [17]. The code uses spline kernel softening, for which the forces become completely Newtonian at 2 softening lengths. Individual time steps for each particle are chosen proportional to the square root of the softening length, ε , over the acceleration, a : $\Delta t_i = \eta \sqrt{\varepsilon/a_i}$. Throughout, we set $\eta = 0.2$, and we keep the value of the softening length constant in comoving coordinates during each run. The physical values of ε at $z = 0$ are listed in Table 1. Forces are computed using terms up to hexadecapole order and a node-opening angle θ which we change from 0.55 initially to 0.7 at $z = 2$. This allows a higher force accuracy when the mass distribution is nearly smooth and the relative force errors can be large. The initial conditions are generated with the GRAFIC2 package ([1]). The starting redshifts z_i are set to the time when the standard deviation of the smallest density fluctuations resolved within the simulation box reaches 0.2 (the smallest scale resolved within the initial conditions is defined as twice the intra-particle distance).

We have set the cosmological parameters according to the fifth-year results of the Wilkinson Microwave Anisotropy Probe mission WMAP5 [8], namely, $\Omega_m = 0.258$, $\Omega_L = 0.742$, $n = 0.963$, $h = 0.72$, and $\sigma_8 = 0.796$, where Ω_m and Ω_L are the values of the density parameters at $z=0$. Table 1 lists all of the simulations used in this work. We have run simulations for several different box sizes, which allows us to probe halo masses covering the entire range $10^{10} h^{-1} M_\odot < M < 10^{15} h^{-1} M_\odot$. In addition, in some cases we have run multiple simulations for the same cosmology and box size, in order to test for the impact of cosmic variance (and to increase the final number of dark matter haloes).

2.2 Halo properties: Concentrations

In this work we identify dark matter halos using a spherical overdensity (SO) algorithm and use a time varying virial density contrast determined using the fitting formula presented in [2]. We include in the halo catalogue all the haloes with more than 500 particles inside the virial radius ($N_{\text{vir}} > 500$).

To compute the concentration of a halo we first determine its density profile. The halo centre is defined as the location of the most bound halo particle (we define the most bound particle as the particle with the lowest potential energy, no care about binding energy is taken here), and we compute the density (ρ_i) in 50 spherical shells, spaced equally in logarithmic radius. Errors on the density are computed from the Poisson noise due to the finite number of particles in each mass shell. The resulting density profile is fitted with a NFW profile:

$$\frac{\rho(r)}{\rho_c} = \frac{\delta_c}{(r/r_s)(1+r/r_s)^2}, \quad (2.1)$$

Name	Box Size	N	m_p	ϵ	$N_{min} > 500$ z=0,2
B20	14.4	250 ³	1.37e7	0.43	974, 1006
B30	21.6	300 ³	2.68e7	0.64	1515, 1399
B40	28.8	250 ³	1.10e8	0.85	1119, 993
B90	64.8	600 ³	9.04e7	0.85	13587, 12177
B180	129.6	300 ³	5.78e9	3.83	2300, 510
B300	216.0	400 ³	1.13e10	4.74	5840, 707
B300 ₂	216.0	400 ³	1.13e10	4.74	5720, 766

Table 1: Table of simulations used in this work. Note that the name of the simulation is related to the box size in units of Mpc. N represents the number of total particles in the box. ϵ represents the force softening length in units of kpc h^{-1} and the last column gives the number of haloes with more than 500 particles at $z = 0$ and $z = 2$. Masses of particles are in units of $h^{-1} M_{\odot}$ and box sizes in units of Mpc h^{-1} , with $h = 0.72$.

During the fitting procedure we treat both r_s and δ_c as free parameters. Their values, and associated uncertainties, are obtained via a χ^2 minimization procedure using the Levenberg & Marquardt method. We define the r.m.s. of the fit as:

$$\rho_{\text{rms}} = \frac{1}{N} \sum_i^N (\ln \rho_i - \ln \rho_m)^2 \quad (2.2)$$

where ρ_m is the fitted NFW density distribution. Finally, we define the concentration of the halo, $c_{\text{vir}} \equiv R_{\text{vir}}/r_s$, using the virial radius obtained from the SO algorithm, and we define the error on $\log c$ as $(\sigma_{r_s}/r_s)/\ln(10)$, where σ_{r_s} is the fitting uncertainty on r_s .

3. Results

In figure 1 we show the median $c_{\text{vir}} - M_{\text{vir}}$ relation for relaxed haloes in our sample at different redshifts. Haloes have been binned in mass bins of 0.4 dex width, the median concentration in each bin has been computed taking into account the error associated to the concentration value (see ??, and M08). In our mass range the $c_{\text{vir}} - M_{\text{vir}}$ relation is well fitted by a single power law at almost all redshifts. Only for $z = 2$ we see an indication that the linearity of the relation in log space seems to break, in agreement with recent findings by [9].

The best fitting power law can be written as:

$$\log(c) = a(z) \log(M_{\text{vir}}/[h^{-1} M_{\odot}]) + b(z) \quad (3.1)$$

The fitting parameters $a(z)$ and $b(z)$ are functions of redshift, the evolution of a and b can be itself fitted with two simple formulas that allow to reconstruct the $c_{\text{vir}} - M_{\text{vir}}$ relation at any redshifts:

$$a(z) = wz - m \quad (3.2)$$

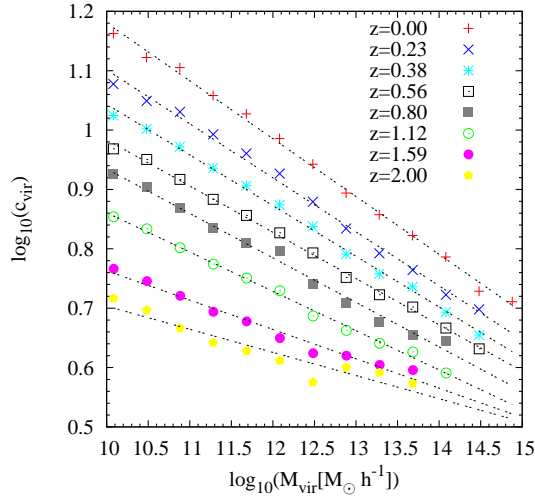


Figure 1: Mass and redshift dependence of the concentration parameter. The points show the median of the concentration as computed from the simulations, averaged for each mass bin. Lines show their respective linear fitting to eq. 3.1.

$$b(z) = \frac{\alpha}{(z + \gamma)} + \frac{\beta}{(z + \gamma)^2} \quad (3.3)$$

Where the additional fitting parameters have been set equal to: $w = 0.029$, $m = 0.097$, $\alpha = -110.001$, $\beta = 2469.720$ and $\gamma = 16.885$. This double fitting formulas are able to recover the original values of the halo concentration with a precision of 5%, for the whole range of masses and redshifts inspected. It has been shown by [18] that using N_{vir} between 100 and 400 particles is enough to get good estimates for the properties of halos, nevertheless in order to look for systematics we re-computed c_{vir} varying the minimum number of particle inside R_{vir} , using 200, 500 and 1000 particles. No appreciable differences (less than 2%) were found in our results for the median.

As can be seen from our results, the mass and redshift dependence of the concentration parameter is considerably different from a simple scaling with redshift [3]. As has been already noted by [19] and [21],[23] the evolution of the concentration parameter is strongly coupled to the growth history of the halo, we will follow this idea to study the physical mechanism behind its evolution. To do so, we built merger trees for all haloes at $z=0$ in our simulations. This time we used haloes with $N_{\text{vir}} > 200$ to be able to follow the evolution of haloes up to earlier times. As was already mentioned, using 200 particles inside the virial radius still gives good results in the estimation of the properties of the halo we are interested in and for simplicity we will only present results from our box B90.

Our methodology is simple, since we define the concentration parameter c_{vir} as the ratio between the virial radius R_{vir} and the scale length radius r_s , we study the evolution of c_{vir} tracking the evolution of these quantities along the merger tree of haloes. It is reasonable to think that the properties of halos we observe at $z=0$ (and at any redshift) are inherited from the most massive progenitor, so we only trace back the properties of the halo along this branch of the tree.

First we explore the relation between M_s , defined as the mass inside r_s , and r_s . Figure 2 shows

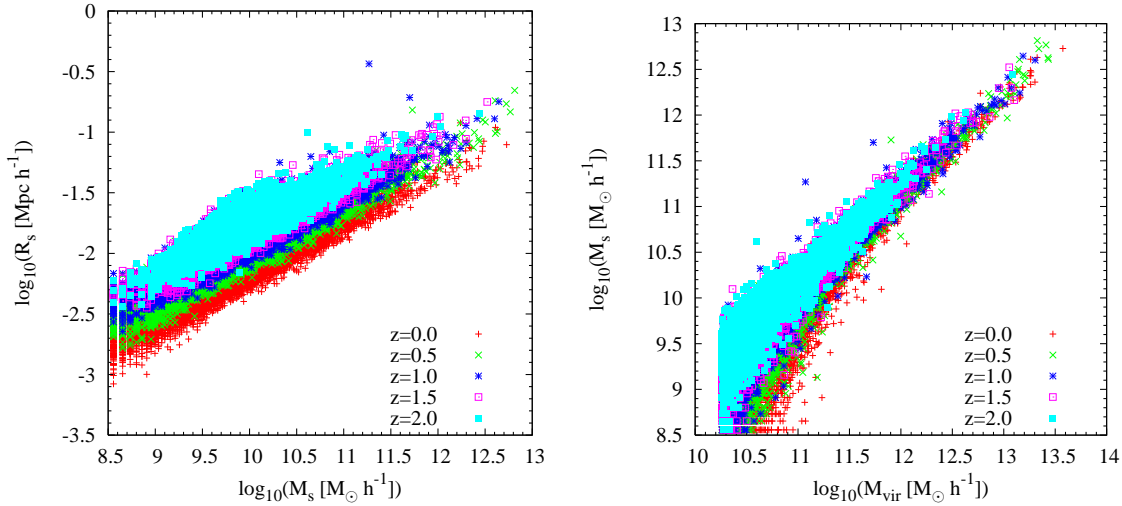


Figure 2: (Left) Relation between M_s and r_s for haloes at different redshift. For all redshifts the mean slope equals 0.38 with very low scatter, while the normalization is clearly redshift dependent. The scatter in the relation is mostly due to the intrinsic scatter in the values of r_s . (Right) Relation between M_{vir} and M_s . Clearly both quantities are directly related with a weak redshift dependence in the normalization.

clearly the relation between both quantities, if $\rho_s(z)$ is the mean mass density inside r_s at a given redshift z , then

$$r_s(z) = \left(\frac{3M_s(z)}{4\pi\rho_s(z)} \right)^\alpha \quad (3.4)$$

if $\rho_s(z)$ were set to be mass independent one could verify that the power index α in 3.4 equals exactly $1/3$, any deviation from that value would be due to a mass dependence on $\rho_s(z)$. The analysis on our data shows robustly that $\alpha \approx 0.38$ close but clearly different from $1/3$, which may imply that $\rho_s(z)$ has a weak dependence on M_s . This behavior can be compared with the one expected from the relation between R_{vir} and M_{vir} where the power index of the equivalent relation 3.4 is exactly $1/3$ without any mass dependence on the mean density of the halo, which is constrained by the values of the overdensity contrast predicted by spherical collapse and the critical density of the universe. Finally, Figure 2 also shows that M_s and M_{vir} are related, so, any dependence of $\rho_s(z)$ with M_s will translate in to a dependence with M_{vir} .

This similarity in the relations between r_s with M_s and R_{vir} with M_{vir} suggest that one may think in an analogous treatment for r_s and M_s as is done for R_{vir} and M_{vir} . Such an analogous analysis is supported by the results of the time evolution of the radial scale length r_s and virial radius R_{vir} along the merger trees. Figure 3 shows the time (redshift) evolution of R_{vir} and r_s . As it can be seen in the figure, the behavior of both quantities show a similar trend. They grow with decreasing redshift, reach a maximum and then start to decrease. The time at which the maximum is reached depends on the final virial mass of the halo, being the low mass ones the firsts reaching that point.

The similarities observed in figures 2 and 3 suggest that one can describe the evolution of the inner region of the halo (the one enclosed by r_s) in a similar way as done for the outer halo. We

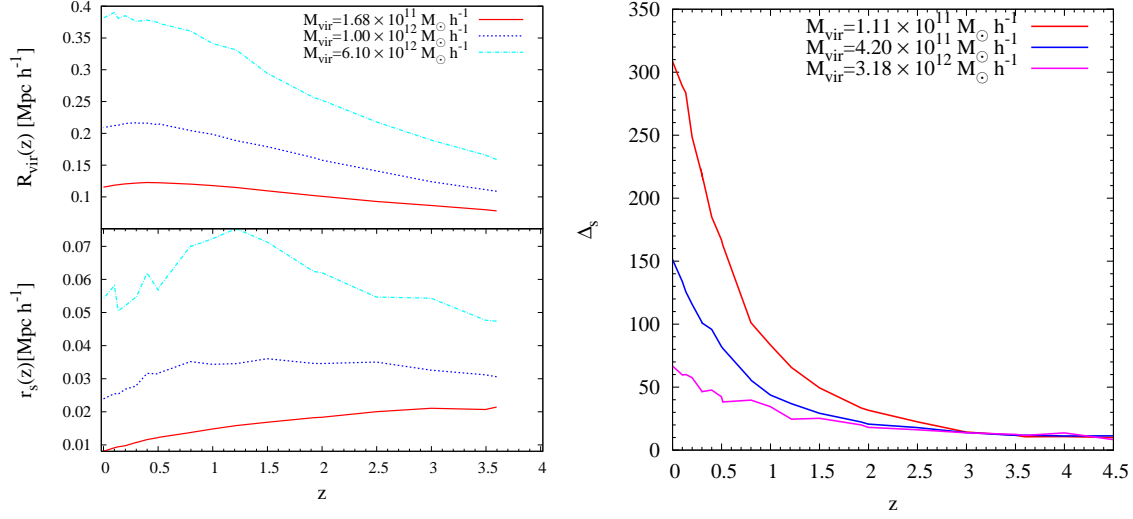


Figure 3: (Left-Top) Time evolution of the virial radius as computed from the averaged merger histories for haloes with final mass of 1.68×10^{11} , 1.0×10^{12} and $6.1 \times 10^{12} h^{-1} M_{\odot}$. (Left-Bottom) Time evolution of the averaged scale length r_s of the dark matter haloes in the same mass bins. (Right) $\Delta_s(z)$ as a function of redshift for three different mass bins computed as the ratio $\rho_s(z)/\rho_{\text{vir}}(z)$ along the merger tree.

assume the inner region of the halo to be a perturbation of mean density $\rho_s(z)$ that evolves within the background of mean density $\rho_{\text{vir}}(z) = \Delta_{\text{vir}}(z)\rho_c(z)$. In analogy with the spherical collapse model we want to look for the evolution of the density contrast of this perturbation: $\Delta_s(z) = \rho_s(z)/\rho_{\text{vir}}(z)$. This inner density contrast is well described by the following formula:

$$\Delta_s(z) = \frac{A}{z + \varepsilon(M)} \quad (3.5)$$

where $A = 50$ and $\varepsilon(M) = 0.3975 \log(M_{\text{vir}}(z=0)/[h^{-1} M_{\odot}]) - 4.312$ best reproduce our data. Equation 3.5 implies that: i) $\rho_s > \rho_{\text{vir}}$ at all redshifts, ii) Δ_s is a growing function of the redshift, implying a fast growth of the inner density with respect to the mean density of the halo and iii) Δ_s depends on the final mass of the halo, and it has lower values for high mass haloes. This mass dependence of Δ_s is also justified from the analysis of figure 2 where it was shown that the mean density of the inner region of the halo must be mass dependent.

One can use all of the previous results to try to reproduce the mean values of the concentration parameter as a function of time for different halo masses. Figure 4 shows the result of modeling c_{vir} after modeling R_{vir} and r_s with the use of eq 3.4. For that $M_{\text{vir}}(z)$ was modeled as a damped exponential law ([14], [13]) and M_s was assumed to follow a power law with M_{vir} with appropriated values for the power law index and normalization.

Although the model works quite well in describing the time dependence of the concentration parameter, it is clear that it works much better for the high mass than for the low mass regime, although for the low mass haloes the model fits very well at high redshift. It is clear that the model performs better for halos in regimes where the nonlinear effects still are not so strong to be predictable by the way spherical collapse approach is implemented in this work.

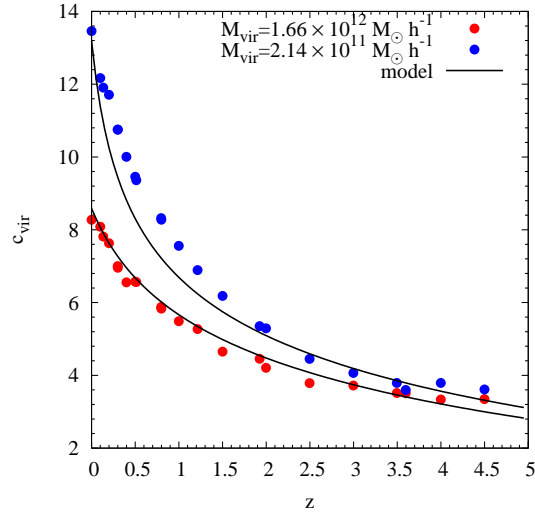


Figure 4: Data and model of the redshift dependence of the concentration parameter. Data points are computed as the ratio between the mean values of R_{vir} and r_s in the respective mass bins along the branch of the most massive progenitors of the tree, the solid lines are the prediction of the model.

4. Conclusions

We present results of the study of the mass and redshift dependence of the concentration parameter of dark matter haloes. In our mass and redshift range the $c_{\text{vir}} - M_{\text{vir}}$ relation always follows a power law behavior. We confirmed that the redshift dependence of such relation is more complex than a simple $(1+z)^{-1}$ scaling as proposed by [3], with both the normalization and the slope of the relation changing with cosmic time. We also found that for increasing redshifts ($z \approx 2$) the power law behavior seems to break, in agreement with recent studies (e.g. [9]). Thanks to our multiple box simulations we tested our results against resolution effects and find them to be stable once a sufficient large number of particles is used $N_{\text{vir}} > 500$.

In order to improve our understanding on the redshift evolution of the $c_{\text{vir}} - M_{\text{vir}}$ relation we look at the individual evolution with time of r_s and R_{vir} . Both these length scales grow with decreasing redshift until a maximum is reached, then they start to decrease towards $z = 0$. There is a clear analogy between the collapse of a linear perturbation and the behavior of r_s and R_{vir} . We found that we can model the evolution of the inner part of the halo as a decoupled spherical perturbation growing inside the central region of the halo. The temporal offset between the “turning points” of the perturbations associated with r_s and R_{vir} is able to explain the observed redshift evolution of the $c_{\text{vir}} - M_{\text{vir}}$ relation. Using this model we presented first results showing that the model we propose may be used to predict the evolution of the halo mass density profile for arbitrary mass and redshifts, which will have important applications in the modeling of the mass distribution of halos in redshift or mass regimes where simulations have limited resolution.

References

- [1] Bertschinger, E. 2001, ApJS, 137, 1

- [2] Bryan, G. L., & Norman, M. L. 1998, *ApJ*, 495, 80
- [3] Bullock, J. S., Kolatt, T. S., Sigad, Y., Somerville, R. S., Kravtsov, A. V., Klypin, A. A., Primack, J. R., & Dekel, A. 2001a, *MNRAS*, 321, 559
- [4] Bullock, J. S., Dekel, A., Kolatt, T. S., Kravtsov, A. V., Klypin, A. A., Porciani, C., & Primack, J. R. 2001b, *ApJ*, 555, 240
- [5] Duffy, A. R., Schaye, J., Kay, S. T., & Dalla Vecchia, C. 2008, *MNRAS*, 390, L64
- [6] Eke, V. R., Navarro, J. F., & Steinmetz, M. 2001, *ApJ*, 554, 114
- [7] Hütsi, G., Hektor, A., & Raidal, M. 2009, *A&A*, 505, 999
- [8] Komatsu E., et al., 2009, *ApJS*, 180, 330
- [9] Klypin, A., Trujillo-Gomez, S., & Primack, J. 2010, arXiv:1002.3660
- [10] Macciò, A. V., Dutton, A. A., van den Bosch, F. C., Moore, B., Potter, D., & Stadel, J. 2007, *MNRAS*, 378, 55
- [11] Macciò, A. V., Dutton, A. A., & van den Bosch, F. C. 2008, *MNRAS*, 391, 1940 (M08)
- [12] Mao, S., Mo, H. J., & White, S. D. M. 1998, *MNRAS*, 297, L71
- [13] Muñoz-Cuertas, J. C., Macciò, A. V., Gottlöber, S., & Dutton, A. A. 2010, *MNRAS*, 1685
- [14] McBride, J., Fakhouri, O., & Ma, C.-P. 2009, *MNRAS*, 398, 1858
- [15] Navarro, J. F., Frenk, C. S., & White, S. D. M. 1997, *ApJ*, 490, 493
- [16] Neto, A. F., et al. 2007, *MNRAS*, 381, 1450
- [17] Stadel, J. G. 2001, Ph.D. Thesis.
- [18] Trenti, M., Smith, B. D., Hallman, E. J., Skillman, S. W., & Shull, J. M. 2010, *ApJ*, 711, 1198
- [19] Wechsler, R. H., Bullock, J. S., Primack, J. R., Kravtsov, A. V., & Dekel, A. 2002, *ApJ*, 568, 52
- [20] White, S. D. M., & Rees, M. J. 1978, *MNRAS*, 183, 341
- [21] Zhao, D. H., Mo, H. J., Jing, Y. P., Börner, G. 2003, *MNRAS*, 339, 12
- [22] Zhao, D. H., Jing, Y. P., Mo, H. J., Börner, G. 2003, *ApJ*, 597, L9
- [23] Zhao, D. H., Jing, Y. P., Mo, H. J., Börner, G. 2009, *ApJ*, 707, 354